ACS APPLIED MATERIALS & INTERFACES

Research Article

www.acsami.org

Enhanced Thermoelectric Performance of Nanostructured Bi_2Te_3 through Significant Phonon Scattering

Lei Yang,[†] Zhi-Gang Chen,*[,†] Min Hong,[†] Guang Han,[†] and Jin Zou*[,†,‡]

[†]Materials Engineering, The University of Queensland, Brisbane, Queensland 4072, Australia

[‡]Centre for Microscopy and Microanalysis, The University of Queensland, Brisbane, Queensland 4072, Australia

ABSTRACT: N-type Bi_2Te_3 nanostructures were synthesized using a solvothermal method and in turn sintered using sparking plasma sintering. The sintered n-type Bi_2Te_3 pellets reserved nanosized grains and showed an ultralow lattice thermal conductivity (~0.2 W m^{-1} K^{-1}), which benefits from high-density small-angle grain boundaries accommodated by dislocations. Such a high phonon scattering leads an enhanced ZT of 0.88 at 400 K. This study provides an efficient method to enhance thermoelectric performance of thermoelectric nanomaterials through nanostructure engineering, making the as-prepared n-type nanostructured Bi_2Te_3 as a promising candidate for room-temperature thermoelectric power generation and Peltier cooling.

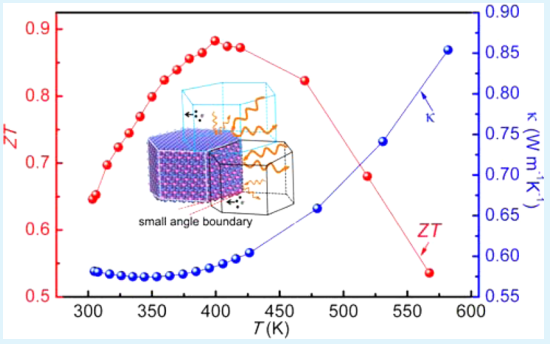

KEYWORDS: *nanostructure engineering, Bi_2Te_3, low thermal conductivity, enhanced thermoelectric properties*

INTRODUCTION

Solid-state thermoelectric cooling and power generation can directly convert between heat and electricity without any emissions or vibrational parts,[1−5] offering the opportunity to overcome the upcoming energy crisis. To achieve high-efficiency energy conversion, extensive progress has been made to improve the thermoelectric performance, which governed by the dimensionless figure-of-merit ZT, defined as $ZT = S^2\sigma T/\kappa = S^2\sigma T/(\kappa_e + \kappa_l)$, where σ is the electrical conductivity, S is the Seebeck coefficient, T is the absolute temperature, and κ is the total thermal conductivity including the contributions from electron (κ_e) and lattice (κ_l).[2,6−8] Intrinsically, an overall high ZT needs a large power factor ($S^2\sigma$), a low κ, or both. However, these transport properties (σ, S, and κ) of thermoelectric materials are highly interdependent and conflicted with each other, which make it a challenge to optimize them to obtain an enhanced ZT.[9−11] Up to now, band engineering, including band convergence,[2] quantum confinement,[12,13] tuning effective mass,[14] and distorting the density of states,[15] have been extensively employed to improve $S^2\sigma$ to achieve a high ZT, while another strategies, such as nanostructure engineering[16,17] or hierarchical architecturing,[6] have been adopted to reduce κ.[18]

As one of the best thermoelectrics at room temperature range,[5,19−25] Bi_2Te_3 is a narrow band gap (~0.15 eV) semiconductor[26] with high valley degeneracy and anisotropic effective mass,[26,27] resulting in an intrinsically high σ and S. Bulk Bi_2Te_3-based materials have been reported with recorded high ZT via introducing doping elements or ternary phase[19,22,28−31] to further increase σ and S, from which the highest $S^2\sigma$ with 4.7× 10^{-3} W m^{-1} K^{-1} has been obtained by doping or alloying Bi_2Te_3 with Se[31] or Sb.[22] However, the relatively high κ of Bi_2Te_3-based bulk materials has become the drawback to achieve higher ZT in bulk materials.[28] Recently, low-dimensional Bi_2Te_3 nanostructures[20,24,25,32] have been developed to target even high ZT according to the theoretical predictions on quantum confinements[12,13,33] to enhance $S^2\sigma$ and nanostructuring to reduce κ_l.[34,35] Additionally, bulk Bi_2Te_3-based materials are anisotropic thermoelectrics,[28,30] while the nanostructured Bi_2Te_3 materials tend to have isotropic properties[20,25] because of the random stacking of nanosized grains. A low $\kappa_l \approx 0.3$ W m^{-1} K^{-1} has been achieved in nanostructured Bi_2Te_3 materials,[17,32] but it is still crucial to clarify the relationship between Bi_2Te_3 microstructure and the increased phonon scattering to fully understand the mechanism of κ_l reduction in nanostructured Bi_2Te_3.

In this study, nanostructure engineering was employed to enhance the thermoelectric performance of nanostructured pure Bi_2Te_3. Plate-like Bi_2Te_3 nanostructures were synthesized via a solvothermal method, and then sintered by sparking plasma sintering (SPS) with a short period of time to avoid grain growth. During the SPS process, a high density of small-angle grain boundaries accommodated by a high-density of dislocations is formed, which strongly scatter the phonons and in turn significantly reducing κ_l. As a consequence, an enhanced ZT with a peak value of 0.88 at ~400 K is obtained from sintered sample. Such a value represents one of the highest reported ZT value for n-type nanostructured pure Bi_2Te_3.

Received: August 17, 2015
Accepted: October 9, 2015
Published: October 9, 2015

DOI: 10.1021/acsami.5b07596
ACS Appl. Mater. Interfaces 2015, 7, 23694−23699

EXPERIMENTAL SECTION

Analytical grade bismuth oxide (Bi_2O_3, 99.9%), tellurium dioxide (TeO_2, 99.999%), sodium hydroxide (NaOH, 99.99%), ethylene glycol, polyvinylpyrrolidone (PVP, average molecular weight = 40 000) were purchased from Sigma-Aldrich and used as precursors without any further purification.

The detailed synthesis procedure is outlined as follows. First, 0.2 g of PVP was dissolved in 18 mL of ethylene glycol to form a clear solution, followed by the additions of 0.2330 g of Bi_2O_3 powders and 0.2396 g of TeO_2 powders. The prepared solution was then mixed with 2 mL of NaOH solution (5 mol/L), the resulting suspension was stirred vigorously for 30 min, and subsequently sealed in a 125 mL Teflon-lined steel autoclave. The autoclave was heated to 210 °C for 24 h and then naturally cooled to room temperature in air. The synthesized products were collected by a high-speed centrifugation, washed by the distilled water and absolute ethanol, and finally dried at 50 °C for at least 12 h.[36,37]

The crystal structures of as-synthesized products and sintered pellets were characterized by X-ray diffraction (XRD), recorded on an X-ray diffractometer (Bruker D8 Advance), equipped with graphite monochromatized, Cu Kα radiation (λ = 1.5418 Å) was used). The morphological, structural, and chemical characteristics of as-synthesized products and sintered pellets were investigated by scanning electron microscopy (SEM, JEOL 7800, operated at 5 kV for normal SEM and 15 kV for backscattered SEM) and transmission electron microscopy (TEM, Philips Tecnai F20, operated at 200 kV).

The as-synthesized Bi_2Te_3 powders were compressed by SPS under 50 MPa and heated at 550 K for 5 min in vacuum. The Archimedes measured were performed to determine the density (d) and relative density (95%) of sintered pellets.

The thermoelectric properties of sintered pellets were studied in both parallel (||) and perpendicular ($\perp$) to the press direction. κ was calculated through $\kappa = DC_pd$, where D and C_p, are the thermal diffusivity and specific heat capacity, respectively. D was measured by a laser flash method with a LFA 457 (NETZSCH). A DSC 404 F3 (NETZSCH) was used to measure C_p. σ and S were measured simultaneously on a ZEM-3 (ULVAC). The uncertainty of the all measurements (S, σ, and D) is estimated as ~5%. The combined uncertainty for the experimental determination of ZT is up to 20%, and the standard deviation of the measured ZT from several different samples is ~3%.

RESULTS AND DISCUSSION

Figure 1a shows a typical XRD pattern of as-synthesized products, which can be indexed exclusively as a rhombohedra structured Bi_2Te_3 phase with lattice parameters of a = 4.386 Å and c = 30.478 Å and a space group of $R\bar{3}m$ (JCPDS 15-0863).[25,36,37] There is no other diffraction peaks can be observed, indicating the high purity of the as-synthesized Bi_2Te_3. Figure 1b is a typical SEM image taken from as-synthesized Bi_2Te_3, in which hexagonal plate-like nanostructures can be observed. The lateral size distributions of these nanostructures are varied from 100 to several hundreds of nanometres. Their typical thickness can be observed in the high magnification SEM (Figure 1c), which is around 20 nm. The crystal structure of Bi_2Te_3 nanoplates are further examined by TEM (Figure 1d, f). Figure 1d is a TEM image of a typical hexagonal-shaped Bi_2Te_3 nanostructure. From the high resolution TEM image (Figure 1e), the measured periodic fringe spacing of 0.22 nm corresponds to the lattice spacing between the $(11\bar{2}0)$ planes, which can be further confirmed by the selected area electron diffraction (SAED) pattern (Figure 1f). The clear lattice fringes in Figure 1e indicate that the nanostructure is well-crystallized.

To measure their thermoelectric properties, the as-synthesized Bi_2Te_3 nanostructures were sintered using SPS to obtain

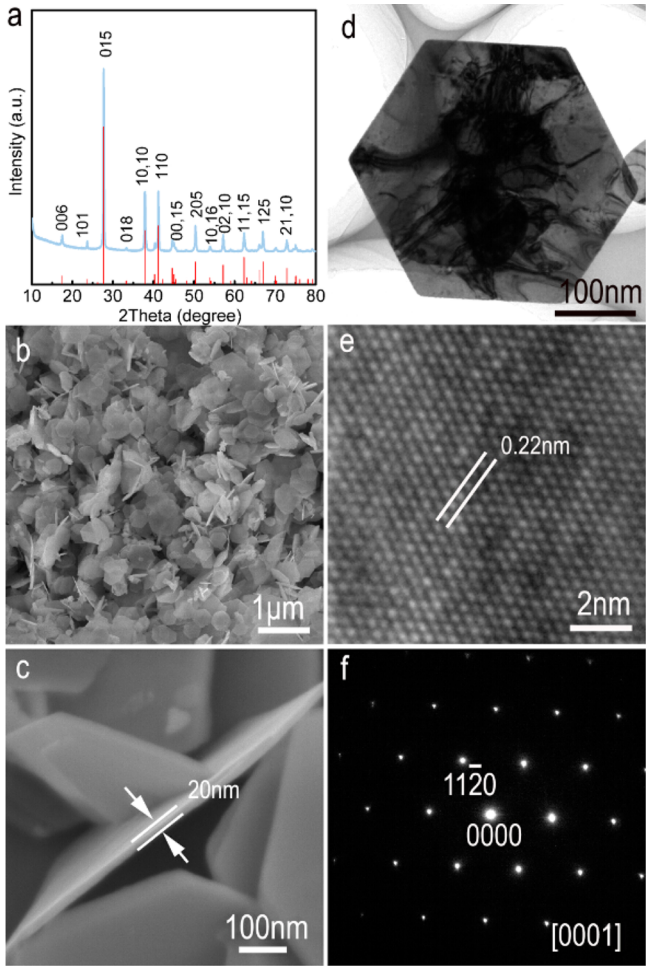

Figure 1. Characterization of as-synthesized Bi_2Te_3 nanostructures: (a) XRD, (b) low magnification SEM image, (c) high magnification SEM showing the thickness of a typical plate-like nanostructure, (d) TEM image, (e) high resolution TEM image, and (f) [0001] zone-axis SAED pattern.

disk-like pellets. Their thermoelectric properties were measured in the temperature range from 300 to 550 K. As mentioned above, the bulk Bi_2Te_3 thermoelectrics showed anisotropy properties. To clarify the nature of isotropy of our nanostructures for their thermoelectric properties, the samples were measured from both parallel (||) and perpendicular ($\perp$) to the press direction. Figure 2 shows various measurement results. As can be seen in Figure 2a, the sintered Bi_2Te_3 shows similar $\sigma_\perp$ and $\sigma_{||}$. The highest σ of 7.2×10^4 S m^{-1} at 300 K is comparable to reported results for pure Bi_2Te_3,[38,39] and then keeps decreasing with increasing the temperature. The measured S (Figure 2b) shows negative values, indicating an n-type pellet. The S values determined from different directions are also isotropic, reached the peak value of -143 μV K^{-1} at ~400 K, which is comparable to the reported results.[38] To obtain κ, D (Figure 2c) and C_p (Figure 2d) were measured. The sintered pellets have similar $D_{||}$ and $D_\perp$, and so for the C_p, leading to similar κ values (Figure 2e). The κ values of sintered pellets are between 0.58 and 0.86 W m^{-1} K^{-1}, which is significantly lower than those of pure Bi_2Te_3,[40,41] but is comparable to the best reported Bi_2Te_3-based materials.[20,32] To investigate κ_e and κ_l, κ_e was calculated using $\kappa_e = L\sigma T$, where L is the Lorenz number.[42] Here, $L = 1.5 \times 10^{-8}$ V^2 K^{-2} is used for estimating κ_e,[38,41] and the obtained κ_e is plotted in Figure 2f.

DOI: 10.1021/acsami.5b07596
ACS Appl. Mater. Interfaces 2015, 7, 23694−23699

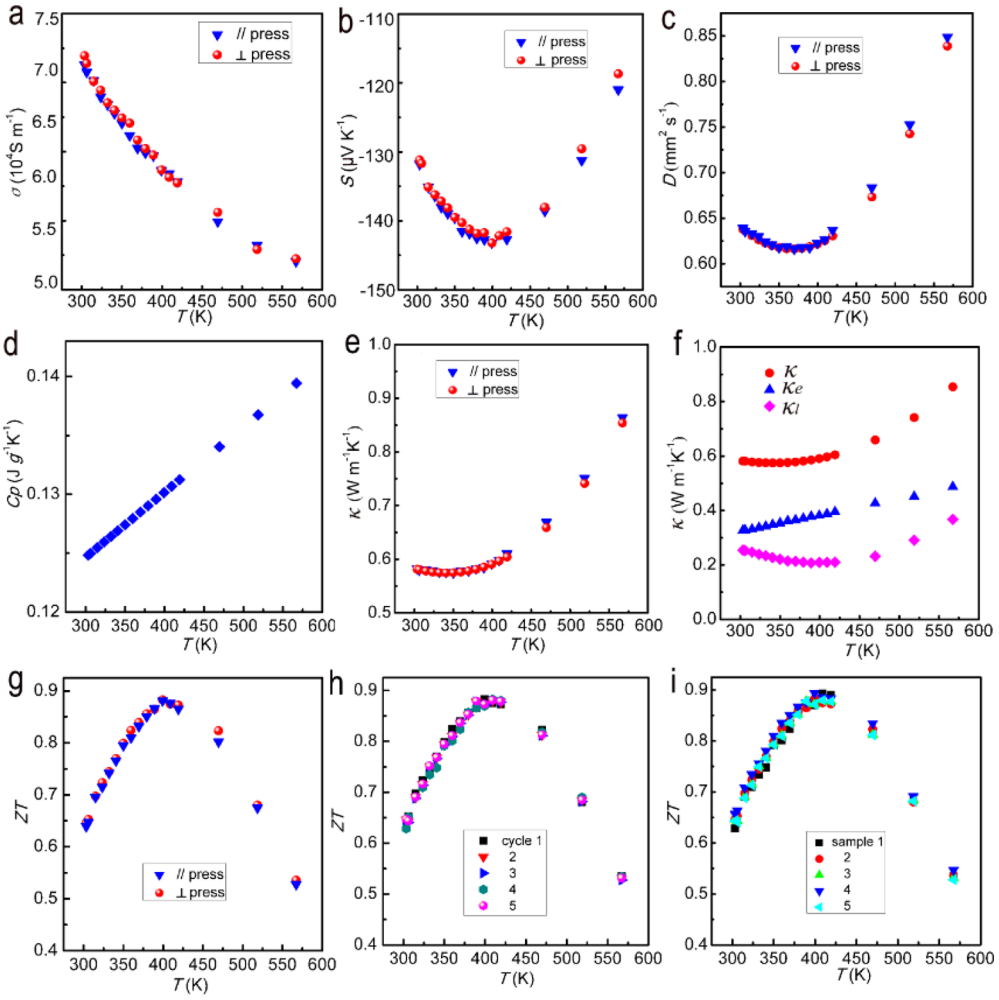

Figure 2. Plots of temperature dependent thermoelectric properties of sintered Bi_2Te_3: (a) Electrical conductivity, (b) Seebeck coefficient, (c) thermal diffusivity, (d) specific heat values, (e) thermal conductivity, (f) κ including the contribution of κ_e and lattice κ_l, (g) calculated ZT values, (h) ZT measured for 5 cycles, and (i) ZT measured for 5 samples.

Using $\kappa_l = \kappa - \kappa_e$, the correspondingly κ_l can be obtained, plotted in Figure 2e. From which, an ultralow κ_l between 0.2 and 0.37 W m^{-1} K^{-1} can be obtained, indicating that the phonons have been strongly scattered. Benefiting from such a low κ, the $ZT_\perp$ reached the peak value of 0.88 at 400 K, while the $ZT_\parallel$ reached almost the same value (Figure 2g). The $ZT_\perp$ value is very stable after several cycles of measurement (as shown in Figure 2h) and similar ZT values can be obtained for 5 different samples (Figure 2i), suggesting that the sintered samples are highly stable and durable.

To understand the fundamental reason for such a low κ_l, detailed structural characterizations were performed on the sintered pellets. Figure 3a is a XRD pattern, which can be again indexed as rhombohedral structured Bi_2Te_3 without any impurities. Figure 3b is a typal SEM image and shows that the nanosized features were preserved in the sintered Bi_2Te_3, and the Bi_2Te_3 nanostructures showed a random stacking with each other. From the backscattered SEM image of the polished sample (Figure 3b inset), no secondary phase and pores can be observed, which confirms that the sintered pellets are high purity and dense. Figure 3c and d are typical TEM images of sintered Bi_2Te_3. Figure 3c shows that Bi_2Te_3 nanostructures can stack to each other with the average thickness of the plate-like grains being approximately 20 nm, resulting in a high density of stacked grains. It should be noted that such a thickness is close to the original Bi_2Te_3 nanoplates, indicating that no significant grain growth occurring during the SPS process. Figure 3d shows nanosized grains with clear gain boundaries, suggesting the random stacking of the Bi_2Te_3 nanostructures in our pellets.

To better understand the structural characteristics at grain boundaries, high-resolution TEM (HRTEM) investigation was employed. Figure 4a is a TEM image showing several grains stacked together. Figure 4b and c are HRTEM images taken from inside a grain and a grain boundary, respectively. Figure 4b shows the grain is well-crystallized with measurable periodicities of lattice spacings of 1 and 0.37 nm, which respectively correspond to the lattice spacing between the (0003) planes and $(10\bar{1}1)$ planes. Figure 4c show a clear grain boundary taken from two adjacent grains with two insets showing the fast Fourier transform (FFT) patterns of the two grains. As can be seen, the upper grain shows clearly lattice image, precisely viewed along the $[11\bar{2}0]$ direction and confirmed by the inset FFT pattern. In contrast, the lattice image of the bottom grain is relatively faint, suggesting there exists misorientation between the two grains, which can be further confirmed by the difference of two inset FFT patterns. Figure 4d is another example, and the inset is the reversed FFT images filtered by ±0001* reflections, in which two dislocations

DOI: 10.1021/acsami.5b07596
ACS Appl. Mater. Interfaces 2015, 7, 23694−23699

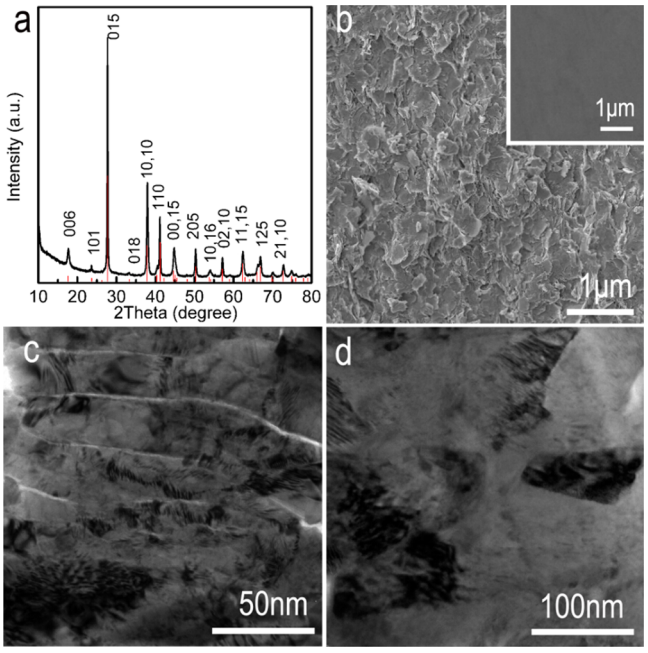

Figure 3. (a) XRD pattern for sintered Bi_2Te_3. (b) SEM image of sintered Bi_2Te_3 with inset of backscattered SEM image of polished sample. (c) TEM image of sintered Bi_2Te_3 showing the stacking of nanosized grains. (d) TEM image of sintered Bi_2Te_3 showing nanosized grains with clear grain boundaries.

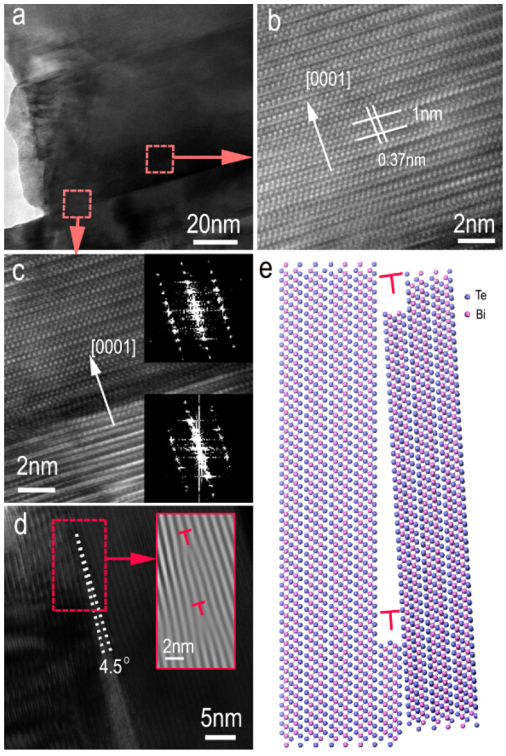

Figure 4. (a) TEM image of sintered Bi_2Te_3 showing nanosized grains and grain boundaries. (b) HRTEM image showing clear crystal lattice within the grain. (c) HRTEM image showing the grain boundary with the inset FFT patterns showing slightly misorientation between two grains. (d) HRTEM image and reversed FFT image showing dislocation cores. (e) Schematic showing the formation of small angle grain boundary with high density of dislocations.

can be clearly seen. A measured misorientation between these grains is about 4.5 degree, which can be believed to belong to small-angle grain boundaries. Their structural model is illustrated by Figure 4e.[43] The observed small grain misorientation should be caused by the stacking of the plate-like nanostructures under high pressure (50 MPa) during the SPS process.

On the basis of above extensive structural characterizations and analysis, we propose a following mechanism for such a low κ, as illustrated in Figure 5. First, as demonstrated in Figure 3, the nanosized Bi_2Te_3 grains have been well preserved without significant grain growth during the sintering process. The stacking of Bi_2Te_3 nanostructures under such a high pressure during the SPS process leads to the formation of a high-density of dislocations accommodated in the small-angle grain boundaries of the sintered Bi_2Te_3 pellets. Such a high density of structural defect features can significantly enhance the phonon scattering in materials.[43,44] In general, the transport of phonons with low, intermediate and high frequencies contribute to the κ_l according to the frequency-dependent description of κ_l.[34] Especially, the intermediate frequency phonons[35] are believed to contribute the most of κ_l.[34] In our sintered Bi_2Te_3 pellets, the existence of fine-grain nanostructures and a high density of dislocations accommodated in a high density of small-angle grain boundaries can strongly block the intermediate frequency and low-frequency phonons with the mean free path of a few hundreds of nanometers or larger,[34,35] to remarkably reduce κ_l and to achieve an overall low κ. It should be noted that point defects often play an important role for the high frequency phonon scattering,[44] and Te_{Bi} antisite defects are often found in the as-prepared Bi_2Te_3 that may contribute to the intrinsic n-type conductivity.[45] Therefore, their contributions should not be ignored. Interestingly, our sintered pellets have shown comparable electrical transport properties with reported Bi_2Te_3 thermoelectrics, indicating that our sample may do not introduce significant change in point defects compared with the reported Bi_2Te_3 thermoelectrics. However, high density small-angle grain boundaries accommodated by a high-density of dislocations were observed in our as-prepared Bi_2Te_3 pellets. As a consequence, we considered that the significantly reduced κ_l found in our pellets should be attributed to these high-density of small-angle grain boundaries accommodated by a high-density of dislocations. As illustrated in Figure 5, the scattering of phonons transition with long and intermediate mean free paths was significantly enhanced by a high-density of small-angle grain boundaries with a high-density of dislocations, providing a full-spectrum phonon scattering nanostructure. Consequently, κ_l is remarkably reduced, which is the major contribution to secure a high ZT in our sintered Bi_2Te_3 nanostructures.

CONCLUSION

In summary, hexagonal plate-like Bi_2Te_3 nanostructures with uniform morphology have been synthesized by using a facile solvothermal method. After the sintering, a high-density of small-angle grain boundaries accommodated by a high density of dislocations is formed due to the stack of plate-like Bi_2Te_3 nanostructures during the SPS process. These structural features reduce the overall κ, and in turn lead to an enhanced ZT of 0.88 at 400 K. This study suggests a strategy to further enhance the phonon scattering of thermoelectric materials to ultimately enhance their thermoelectric performances.

DOI: 10.1021/acsami.5b07596
ACS Appl. Mater. Interfaces 2015, 7, 23694−23699

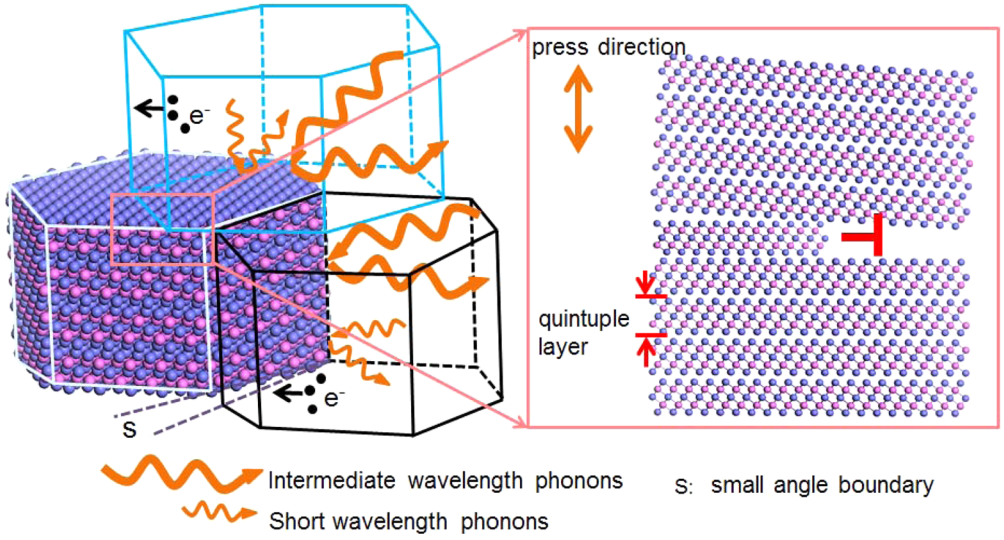

Figure 5. Schematics of the phonon scattering mechanism for sintered Bi_2Te_3.

AUTHOR INFORMATION

Corresponding Authors

*Email: z.chen1@uq.edu.au.

* Email: j.zou@uq.edu.au.

Notes

The authors declare no competing financial interest.

ACKNOWLEDGMENTS

This work was financially supported by the Australian Research Council. Z.-G.C. thanks QLD government for a smart state future fellowship (2011002414). L.Y. thanks the China Scholarship Council for providing his PhD stipend. The Australian Microscopy & Microanalysis Research Facility and the Queensland node of the Australian National Fabrication Facility are acknowledged for providing characterization facilities.

REFERENCES

(1) Chen, Z. G.; Han, G.; Yang, L.; Cheng, L.; Zou, J. Nanostructured Thermoelectric Materials: Current Research and Future Challenge. *Prog. Nat. Sci.* **2012**, *22*, 535−549.

(2) Pei, Y. Z.; Shi, X. Y.; LaLonde, A.; Wang, H.; Chen, L. D.; Snyder, G. J. Convergence of Electronic Bands for High Performance Bulk Thermoelectrics. *Nature* **2011**, *473*, 66−69.

(3) Zhao, L.-D.; Lo, S.-H.; Zhang, Y.; Sun, H.; Tan, G.; Uher, C.; Wolverton, C.; Dravid, V. P.; Kanatzidis, M. G. Ultralow Thermal Conductivity and High Thermoelectric Figure of Merit in SnSe Crystals. *Nature* **2014**, *508*, 373−377.

(4) Snyder, G. J.; Toberer, E. S. Complex Thermoelectric Materials. *Nat. Mater.* **2008**, *7*, 105−114.

(5) Tritt, T. M. Thermoelectric Materials - Holey and Unholey Semiconductors. *Science* **1999**, *283*, 804−805.

(6) Biswas, K.; He, J.; Blum, I. D.; Wu, C.-I.; Hogan, T. P.; Seidman, D. N.; Dravid, V. P.; Kanatzidis, M. G. High-performance Bulk Thermoelectrics with All-scale Hierarchical Architectures. *Nature* **2012**, *489*, 414−8.

(7) Venkatasubramanian, R.; Siivola, E.; Colpitts, T.; O'Quinn, B. Thin-film Thermoelectric Devices with High Room-temperature Figures of Merit. *Nature* **2001**, *413*, 597−602.

(8) Hsu, K. F.; Loo, S.; Guo, F.; Chen, W.; Dyck, J. S.; Uher, C.; Hogan, T.; Polychroniadis, E. K.; Kanatzidis, M. G. Cubic $AgPb_mSbTe_{2+m}$: Bulk Thermoelectric Materials with High Figure of Merit. *Science* **2004**, *303* (5659), 818−821.

(9) Yang, J.; Yip, H. L.; Jen, A. K. Y. Rational Design of Advanced Thermoelectric Materials. *Adv. Energy Mater.* **2013**, *3*, 549−556.

(10) Zebarjadi, M.; Esfarjani, K.; Dresselhaus, M. S.; Ren, Z. F.; Chen, G. Perspectives on Thermoelectrics: From Fundamentals to Device Applications. *Energy Environ. Sci.* **2012**, *5*, 5147−5162.

(11) Rowe, D. M. In *Thermoelectrics Handbook: Macro to Nano*; Rowe, D. M., Ed.; CRC Press: Boca Raton, FL, 2005; Chapter 1, pp 1−14.

(12) Hicks, L. D.; Harman, T. C.; Dresselhaus, M. S. Use of Quantum-well Superlattices to Obtain a High Figure of Merit From Nonconventional Thermoelectric Materials. *Appl. Phys. Lett.* **1993**, *63*, 3230−3232.

(13) Molenkamp, L. W.; Van Houten, H.; Staring, A. A. M.; Beenakker, C. W. J. Quantum Effects in Thermal and Thermoelectric Transport in Semiconductor Nanostructures. *Phys. Scr.* **1993**, *T49b*, 441−445.

(14) Pei, Y.; Wang, H.; Snyder, G. J. Band Engineering of Thermoelectric Materials. *Adv. Mater.* **2012**, *24*, 6125−35.

(15) Rhyee, J. S.; Lee, K. H.; Lee, S. M.; Cho, E.; Il Kim, S.; Lee, E.; Kwon, Y. S.; Shim, J. H.; Kotliar, G. Peierls Distortion as A Route to High Thermoelectric Performance in In_4Se_3-Delta Crystals. *Nature* **2009**, *459*, 965−968.

(16) Zhu, H.-T.; Luo, J.; Liang, J.-K. Synthesis of Highly Crystalline Bi_2Te_3 Nanotubes and Their Enhanced Thermoelectric Properties. *J. Mater. Chem. A* **2014**, *2*, 12821−12826.

(17) Wan, C. L.; Wang, Y. F.; Wang, N.; Norimatsu, W.; Kusunoki, M.; Koumoto, K. Development of Novel Thermoelectric Materials by Reduction of Lattice Thermal Conductivity. *Sci. Technol. Adv. Mater.* **2010**, *11*, 044306.

(18) Ma, Y.; Hao, Q.; Poudel, B.; Lan, Y. C.; Yu, B.; Wang, D. Z.; Chen, G.; Ren, Z. F. Enhanced Thermoelectric Figure-of-merit in p-type Nanostructured Bismuth Antimony Tellurium Alloys Made From Elemental Chunks. *Nano Lett.* **2008**, *8*, 2580−2584.

(19) Son, J. S.; Choi, M. K.; Han, M. K.; Park, K.; Kim, J. Y.; Lim, S. J.; Oh, M.; Kuk, Y.; Park, C.; Kim, S. J.; Hyeon, T. n-Type Nanostructured Thermoelectric Materials Prepared from Chemically Synthesized Ultrathin Bi_2Te_3 Nanoplates. *Nano Lett.* **2012**, *12*, 640−647.

(20) Harman, T. C.; Taylor, P. J.; Walsh, M. P.; LaForge, B. E. Quantum Dot Superlattice Thermoelectric Materials and Devices. *Science* **2002**, *297*, 2229−2232.

(21) Poudel, B.; Hao, Q.; Ma, Y.; Lan, Y. C.; Minnich, A.; Yu, B.; Yan, X.; Wang, D. Z.; Muto, A.; Vashaee, D.; Chen, X. Y.; Liu, J. M.; Dresselhaus, M. S.; Chen, G.; Ren, Z. High-thermoelectric Performance of Nanostructured Bismuth Antimony Telluride Bulk Alloys. *Science* **2008**, *320*, 634−638.

DOI: 10.1021/acsami.5b07596
ACS Appl. Mater. Interfaces 2015, 7, 23694−23699

(22) Scherrer, S.; Scherrer, H. In *Thermoelectrics Handbook: Macro to Nano*; Rowe, D. M.; CRC Press: Boca Raton, FL, 2005; Chapter 27, pp 1−19.
(23) Han, G.; Chen, Z.-G.; Yang, L.; Hong, M.; Drennan, J.; Zou, J. Rational Design of Bi_2Te_3 Polycrystalline Whiskers for Thermoelectric Applications. *ACS Appl. Mater. Interfaces* **2015**, *7*, 989−995.
(24) Cheng, L.; Chen, Z. G.; Yang, L.; Han, G.; Xu, H. Y.; Snyder, G. J.; Lu, G. Q.; Zou, J. T-Shaped Bi_2Te_3−Te Heteronanojunctions: Epitaxial Growth, Structural Modeling, and Thermoelectric Properties. *J. Phys. Chem. C* **2013**, *117*, 12458−12464.
(25) Greenaway, D. L.; Harbeke, G. Band Structure of Bismuth Telluride Bismuth Selenide and Their Respective Alloys. *J. Phys. Chem. Solids* **1965**, *26*, 1585−1604.
(26) Mishra, S. K.; Satpathy, S.; Jepsen, O. Electronic Structure and Thermoelectric Properties of Bismuth Telluride and Bismuth Selenide. *J. Phys.: Condens. Matter* **1997**, *9*, 461−470.
(27) Yan, X.; Poudel, B.; Ma, Y.; Liu, W. S.; Joshi, G.; Wang, H.; Lan, Y.; Wang, D.; Chen, G.; Ren, Z. F. Experimental Studies on Anisotropic Thermoelectric Properties and Structures of n-Type $Bi_2Te_{2.7}Se_{0.3}$. *Nano Lett.* **2010**, *10*, 3373−3378.
(28) Zhai, Y.; Zhang, T.; Xiao, Y.; Jiang, J.; Yang, S.; Xu, G. Enhanced Thermoelectric Performance in n-type $Bi_2Te_{2.994}Cl_{0.006}/In_2Te_3$ Composite. *J. Alloys Compd.* **2013**, *563*, 285−288.
(29) Liu, W.-S.; Zhang, Q.; Lan, Y.; Chen, S.; Yan, X.; Zhang, Q.; Wang, H.; Wang, D.; Chen, G.; Ren, Z. Thermoelectric Property Studies on Cu-Doped n-type $Cu_xBi_2Te_{2.7}Se_{0.3}$ Nanocomposites. *Adv. Energy Mater.* **2011**, *1*, 577−587.
(30) Carle, M.; Pierrat, P.; Lahalle-Gravier, C.; Scherrer, S.; Scherrer, H. Transport Properties of n-type $Bi_2(Te_{1-x}Se_x)_3$ Single Crystal Solid Solutions ($x \leqslant 0.05$). *J. Phys. Chem. Solids* **1995**, *56*, 201−209.
(31) Mehta, R. J.; Zhang, Y. L.; Karthik, C.; Singh, B.; Siegel, R. W.; Borca-Tasciuc, T.; Ramanath, G. A New Class of Doped Nanobulk High-figure-of-merit Thermoelectrics by Scalable Bottom-up Assembly. *Nat. Mater.* **2012**, *11*, 233−240.
(32) Hicks, L. D.; Harman, T. C.; Sun, X.; Dresselhaus, M. S. Experimental Study of The Effect of Quantum-well Structures on The Thermoelectric Figure of Merit. *Phys. Rev. B: Condens. Matter Mater. Phys.* **1996**, *53*, 10493−10496.
(33) Toberer, E. S.; Zevalkink, A.; Snyder, G. J. Phonon Engineering Through Crystal Chemistry. *J. Mater. Chem.* **2011**, *21*, 15843−15852.
(34) Chen, G.; Dames, C. In *Thermoelectrics Handbook: Macro to Nano*; Rowe, D. M.; CRC Press: Boca Raton, FL, 2005; Chapter 42, pp 1−16.
(35) Chen, Z.-G.; Yang, L.; Ma, S.; Cheng, L.; Han, G.; Zhang, Z.-d.; Zou, J. Paramagnetic Cu-doped Bi_2Te_3 Nanoplates. *Appl. Phys. Lett.* **2014**, *104*, 053105.
(36) Cheng, L.; Chen, Z. G.; Ma, S.; Zhang, Z. D.; Wang, Y.; Xu, H. Y.; Yang, L.; Han, G.; Jack, K.; Lu, G. Q.; Zou, J. High Curie Temperature $Bi_{1.85}Mn_{0.15}Te_3$ Nanoplates. *J. Am. Chem. Soc.* **2012**, *134*, 18920−18923.
(37) Zhao, X. B.; Ji, X. H.; Zhang, Y. H.; Zhu, T. J.; Tu, J. P.; Zhang, X. B. Bismuth Telluride Nanotubes and The Effects on The Thermoelectric Properties of Nanotube-containing Nanocomposites. *Appl. Phys. Lett.* **2005**, *86*, 062111.
(38) Tang, X.; Xie, W.; Li, H.; Zhao, W.; Zhang, Q.; Niino, M. Preparation and Thermoelectric Transport Properties of High-performance p-type Bi_2Te_3 with Layered Nanostructure. *Appl. Phys. Lett.* **2007**, *90*, 012102.
(39) Zhang, Y.; Wang, H.; Kräemer, S.; Shi, Y.; Zhang, F.; Snedaker, M.; Ding, K.; Moskovits, M.; Snyder, G. J.; Stucky, G. D. Surfactant-Free Synthesis of Bi_2Te_3−Te Micro−Nano Heterostructure with Enhanced Thermoelectric Figure of Merit. *ACS Nano* **2011**, *5*, 3158−3165.
(40) Zhao, X. B., In *Thermoelectrics Handbook: Macro to Nano*; Rowe, D. M.; CRC Press: Boca Raton, FL, 2005; Chapter 25, pp 1−10.
(41) Liu, H.; Shi, X.; Xu, F.; Zhang, L.; Zhang, W.; Chen, L.; Li, Q.; Uher, C.; Day, T.; Snyder, G. J. Copper Ion Liquid-like Thermoelectrics. *Nat. Mater.* **2012**, *11*, 422−425.
(42) Kim, S. I.; Lee, K. H.; Mun, H. A.; Kim, H. S.; Hwang, S. W.; Roh, J. W.; Yang, D. J.; Shin, W. H.; Li, X. S.; Lee, Y. H.; Snyder, G. J.; Kim, S. W. Dense Dislocation Arrays Embedded in Grain Boundaries for High-performance Bulk Thermoelectrics. *Science* **2015**, *348*, 109−114.
(43) Medlin, D. L.; Snyder, G. J. Interfaces in Bulk Thermoelectric Materials a Review for Current Opinion in Colloid and Interface Science. *Curr. Opin. Colloid Interface Sci.* **2009**, *14*, 226−235.
(44) Callaway, J.; von Baeyer, H. C. Effect of Point Imperfections on Lattice Thermal Conductivity. *Phys. Rev.* **1960**, *120*, 1149−1154.
(45) Hashibon, A.; Elsasser, C. First-principles Density Functional Theory Study of Native Point Defects in Bi_2Te_3. *Phys. Rev. B: Condens. Matter Mater. Phys.* **2011**, *84*, 144117.

DOI: 10.1021/acsami.5b07596
ACS Appl. Mater. Interfaces 2015, 7, 23694−23699